

Performance Assessment of MIMO Precoding on Realistic mmWave Channels

*Mattia Rebato, [†]Luca Rose, *Michele Zorzi

*Department of Information Engineering, University of Padova, 35131 Padova, Italy

[†]Nokia Bell Labs, Paris – Saclay, France

{rebato, zorzi}@dei.unipd.it – luca.rose@nokia-bell-labs.com

Abstract—In this paper, the performance of multi-user Multiple-Input Multiple-Output (MIMO) systems is evaluated in terms of SINR and capacity. We focus on the case of a downlink single-cell scenario where different precoders have been studied. Among the considered precoders, we range from different Grid of Beams (GoB) optimization approaches to linear precoders (e.g., matched filtering and zero forcing). This performance evaluation includes imperfect channel estimation, and is carried out over two realistic mmWave 5G propagation channels, which are simulated following either the measurement campaign done by New York University (NYU) or the 3GPP channel model. Our evaluation allows grasping knowledge on the precoding performance in mmWave realistic scenarios. The results highlight the good performance of GoB optimization approaches when a realistic channel model with directionality is adopted.

Index Terms—Millimeter-wave, multi-user MIMO, 5G, interference optimization, linear precoder, grid of beams.

I. INTRODUCTION

The volume of mobile data is continuously increasing, especially with high capacity applications that are emerging together with the next generation (i.e., 5G) of cellular communications [1]. As an enabler for these capacity-intensive applications, the millimeter wave (mmWave) band (approximately between 10 and 300 GHz) has been identified as a promising candidate for future mobile communications [2]. In addition to the use of mmWave frequencies, another major aspect of the new mobile generation is the densification of the network applying small cells in large numbers. Furthermore, Multi-User (MU) massive Multiple-Input Multiple-Output (MIMO) systems became of high interest as they contribute to reaching the 5G high demands (e.g., in terms of rates and densities), due to their ability to greatly increase network capacity [3]. For this reason, it is important to study and evaluate MU massive MIMO systems over 5G mmWave propagation channels. By exploiting such technologies, data transmission rates are expected to increase in the Radio Access Network (RAN), and a more efficient use of the radio spectrum can be achieved.

The purpose of MU MIMO systems is to account for channel scattering and reflections, thus exploiting the spatial dimension and creating multiple beams of the signal in the direction of the User Equipments (UEs), so that each user can benefit from the whole allowed bandwidth at any time instant. This can be achieved by precoding the information at the Next Generation Node Base (gNB) side. Using a precoder, data is distributed on the different antenna elements of the

gNB in order to perform beamforming of information toward the served UEs.

Many works in the literature focused on the evaluation of precoding techniques for MU mmWave systems with massive MIMO. The closest works to ours are [4]–[7]. In [4], massive MIMO was proposed and studied under the ideal condition of almost infinite antennas. In [5], precoding techniques such as Minimum Mean Square Error (MMSE), Matched Filtering (MF) and Zero Forcing (ZF) were studied under the assumption of a Rayleigh channel model and under the condition of perfect Channel State Information (CSI) acquisition. In [6], channel estimation errors were introduced to estimate the implementation loss in terms of precoding gain, whereas in [7] the authors link the precoding performance with channel correlation. Finally, a recent piece of work [8] uses a realistic channel model to perform an evaluation of a MU system in terms of bit error rate as a function of the number of antenna elements used at the transmitter side, while however overlooking the effect of different precoding strategies and channel estimation errors.

From the literature, it emerges that linear precoding schemes can be used to reach high performance under ideal assumptions. Less known is however their performance when realistic channel models are considered. To be precise, under a Rayleigh fading model, it is known that MMSE performs appreciably better in terms of balancing the resources among the UEs acting as a trade-off between MF and ZF approaches. However, the Rayleigh fading model oversimplifies the channel characterization, resulting in a channel model that does not reflect the real mmWave propagation specifics.

In 3GPP NR systems, the exploitation of mmWave frequency bands (both at 28 GHz and at 60 GHz) for the next generation of mobile communications is currently defined [9]. Within the standard, different types of CSI feedback mechanisms have been included to support MIMO transmissions. In particular, release 15 includes Type-I and Type-II codebook CSI feedback, enabling different trade-offs between CSI resolutions and feedback overhead [10]. More precisely, when a Type-I CSI feedback scheme is adopted, the UE feeds back the index of a vector taken from a suitable oversampled DFT codebook that best approximates the dominant eigenvector of the channel matrix; conversely, when Type-II CSI is adopted, the feedback is composed of a linear combination of two or more (up to 4 per polarization) vectors taken from the oversampled

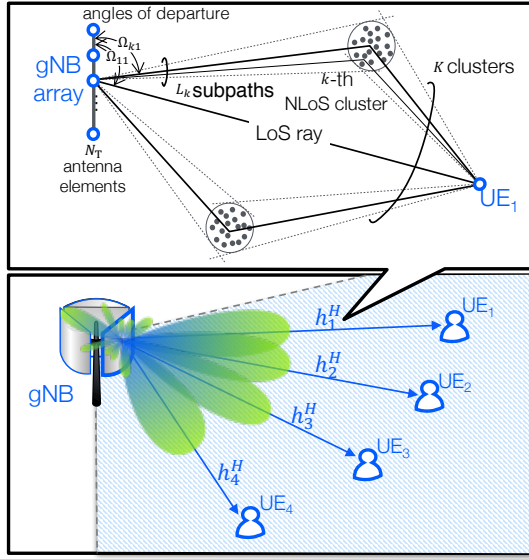


Figure 1: Illustration of the mmWave system model considered (bottom) and representation of the channel model used for each link in the framework (top).

DFT codebook. In this latter case, both the indices of the chosen vectors and the linear combination coefficients are fed back to gNB. Finally, it is worth observing that the accuracy of a Type-II CSI feedback scheme is larger, and so is the resulting overhead [11]. The reason behind such mechanisms is to be found in the attempt to reduce the amount of CSI acquisition overhead while exploiting MIMO advantages, such as spatial multiplexing and beamforming. Although at the moment full CSI¹ is not included in the standard, ongoing discussions are attempting to assess the trade-off between precoding gain and overhead cost.

Differently from the prior art, the objective of this study is twofold. First, we aim at evaluating the performance of diverse precoders when a realistic channel is considered, where “realistic” denotes both the adoption of a channel model supported by experimental evidence and the inclusion of CSI imperfections. Second, we compare the aforementioned linear precoders against Grid of Beams (GoB) optimization approaches, with the goal of assessing the gain of linear precoders over simpler (and less demanding in term of CSI) GoB approaches.

As reported in Figure 1, we consider a scenario with both a realistic sectorization and an antenna array radiation pattern, as suggested by the 3GPP specifications in [12]. Moreover, two measurement-based realistic channel models are considered, one from New York University (NYU) [13] and one from 3GPP as suggested in [14], both used to evaluate and compare the performance of different precoders.

Notation: In this paper, column vectors and matrices are respectively denoted by boldface lowercase and uppercase letters. We identify with \mathbf{X}^H the conjugate transpose of \mathbf{X} , and the Frobenius norm is denoted $\|\cdot\|_F$ while the Euclidean norm is denoted as $\|\cdot\|$. The set of all complex numbers is denoted

by \mathbb{C} , with $\mathbb{C}^{N \times 1}$ and $\mathbb{C}^{N \times M}$ being the generalizations to vectors and matrices, respectively. The $M \times M$ identity matrix is written as \mathbf{I}_M and the zero matrix of size $N_T \times M$ is denoted as $\mathbf{0}_{N_T \times M}$. Finally, we generally indicate with $\hat{\mathbf{X}}$ the Frobenius normalized matrix of \mathbf{X} .

II. SYSTEM MODEL

We consider a narrowband single-cell downlink multi-user MIMO mmWave system where a single gNB sector with N_T transmit antennas is serving M single-antenna UEs.² The channel to the m -th user is assumed narrowband and is described by the vector of coefficients $\mathbf{h}_m \in \mathbb{C}^{N_T \times 1}$, and its j -th element describes the channel response between the j -th transmitting antenna element and the receive antenna. This input-output relationship can be described as

$$y_m = \mathbf{h}_m^H \mathbf{x} + n_m, \quad m \in \{1, 2, \dots, M\} \quad (1)$$

where \mathbf{x} is the $N_T \times 1$ transmitted vector signal, $y_m \in \mathbb{C}$ is the received signal, and n_m is the noise term. Assuming to use a precoder, the transmitted vector signal is $\mathbf{x} = \sum_{i=1}^M \mathbf{w}_i s_i$, where s_i is the data symbol and \mathbf{w}_i is the $N_T \times 1$ linear precoding vector.

Aggregating together the precoding vectors of all the M UEs we can define the precoding matrix $\mathbf{W} = [\mathbf{w}_1, \dots, \mathbf{w}_M] \in \mathbb{C}^{N_T \times M}$. We note that, in order to respect the power constraint $\mathbb{E}[\|\mathbf{W}\mathbf{s}\|^2] = 1$, we normalize the precoding matrix with the Frobenius norm as follows $\hat{\mathbf{W}} = \frac{\mathbf{W}}{\|\mathbf{W}\|_F}$. Using this notation, it is possible to write the system input-output equation as

$$\mathbf{y} = \mathbf{H}^H \hat{\mathbf{W}} \mathbf{s} + \mathbf{n} \quad (2)$$

where \mathbf{y}, \mathbf{s} and \mathbf{n} are vectors with dimension $M \times 1$, while channel matrix \mathbf{H} is defined in $\mathbb{C}^{N_T \times M}$.

Finally, we define $\bar{\mathbf{H}}^{(p)}$ as the $M \times M$ equivalent matrix obtained with the product

$$\bar{\mathbf{H}}^{(p)} = \mathbf{H}^H \hat{\mathbf{W}}^{(p)} \quad (3)$$

where superscript p is used to identify the different precoding approaches evaluated as described in the following.

A. Channel Models

In our evaluation, MIMO channel vectors \mathbf{h} are generated according to three distinct statistical channel models. The first model under analysis is a standard Rayleigh fading channel model; the second is derived from a set of extensive measurement campaigns in New York City by NYU-Wireless [13]; the last model considered is the one provided by the 3GPP [14], which was obtained from multiple measurement campaigns from different research groups all around the world. For this study, we adopt the channel model with the settings of the Urban Macro (UMa) scenario.

Both the realistic models (i.e., NYU and 3GPP) are based on the WINNER II channel characterization [15], and consider

¹According to the 3GPP terminology, the term full CSI is known as explicit CSI.

²We note that the number of UEs that can be simultaneously supported by the gNB sector is less than or equal to the number of antenna elements, i.e., $M \leq N_T$.

macro-level scattering paths and sub-paths. Some minor differences are present in the settings of the models, nevertheless, a major difference is identified in the number of paths and sub-paths considered. The NYU characterization has higher *directionality* obtained by assuming a smaller number of paths. To be precise, the NYU model considered a maximum of 4 main paths (defined as *clusters*), while the 3GPP channel model can reach a maximum of 20 clusters in Non Line of Sight (NLoS) conditions. Here, by *directionality*, we mean the ability of the channel and beamforming, to focus the power in a specific direction. Together with the channel, also a measurement-based distance-dependent path loss model is considered with Line of Sight (LoS), NLoS and outage conditions.

At the transmitter side, we model the antenna of the considered sector as a Uniform Planar Array (UPA). In this manner, the beamforming can be performed in both the azimuth and elevation dimensions. Furthermore, we precisely model each element radiation pattern following the 3GPP specifications in [12] and [14], as done in our previous work [16]. We consider the superposition of element radiation pattern and array factor in order to gather a precise knowledge of the array radiation effects due to beamforming. This permits a careful characterization of the steering beams, and therefore a precise knowledge of the amount of power irradiated by the antenna array in all directions. Thus, we are realistically computing both the desired and the interfering signals. A complete explanation of the relationship between array and element patterns can be found in [12] and [16].

The channel of each link is computed with a set of K clusters and L_k sub-paths per cluster (as shown in the top part of Figure 1), and is represented as

$$\mathbf{h} = \sum_{k=1}^K \sum_{l=1}^{L_k} g_{kl} \mathbf{F}_T(\Omega_{kl}) \mathbf{u}_T(\Omega_{kl}) \quad (4)$$

where g_{kl} is the small-scale fading gain of sub-path l in cluster k , and \mathbf{u}_T is the 3D spatial signature vector of the transmitter. Furthermore, for brevity, we use subscript or superscript T, referring to a transmitter related term. Moreover, $\Omega_{kl} = (\theta_{kl}, \phi_{kl})$ is the angular spread of vertical and horizontal Angles of Departure (AoD) for sub-path l in cluster k [13]. Finally, \mathbf{F}_T is the field factor term of the transmitting array. Detailed explanation on how to precisely compute all these channel terms can be found in [13] and [16].

B. Precoders Considered

With the intent to perform a study of the different precoding techniques while realistically modeling the channel, we discuss in the following paragraphs all the approaches evaluated and provide details on how they are computed.

a) Grid of beams (power optimization): This approach consists in the use of a codebook \mathcal{Z} of precomputed precoders that will be tested with the aim to choose the one that maximizes a specific metric. Each precoder vector in the codebook represents a Discrete Fourier Transform (DFT) beam

pointing towards a direction. According to this principle, the entire codebook spans the whole effective area.³

Two different GoB metrics and thus optimization criteria are considered in this study. First, for each active UE, we identify the precoder $\mathbf{w}_m^{(\text{GoB}_P)}$ which maximizes the received power among all possible precoder vectors z in the codebook \mathcal{Z} , thus

$$\mathbf{w}_m^{(\text{GoB}_P)} = \arg \max_{z \in \mathcal{Z}} |\mathbf{h}_m^H \mathbf{w}_z|^2. \quad (5)$$

We identify it with the acronym GoB_P, and the respective precoding matrix is derived as

$$\mathbf{W}^{(\text{GoB}_P)} = [\mathbf{w}_1^{(\text{GoB}_P)}, \dots, \mathbf{w}_M^{(\text{GoB}_P)}]. \quad (6)$$

b) Grid of beams (SLNR optimization): Similarly, we study an alternative in which the precoder is chosen by maximizing the Signal to Leakage plus Noise Ratio (SLNR) for each single UE m . We define it as GoB_{SLNR} and the optimization expression becomes

$$\mathbf{w}_m^{(\text{GoB}_{\text{SLNR}})} = \arg \max_{z \in \mathcal{Z}} \left(\frac{|\mathbf{h}_{m,m}^H \mathbf{w}_z|^2}{\sigma^2 + \sum_{i \neq m} |\mathbf{h}_{m,i}^H \mathbf{w}_z|^2} \right) \quad (7)$$

then, the precoder matrix $\mathbf{W}^{(\text{GoB}_{\text{SLNR}})}$ is derived as in (6).

The rationale behind this choice is that the sum of SLNRs is a close approximation of the sum of Signal to Interference plus Noise Ratios (SINRs), with the advantage of being computationally much easier to perform. This stems mainly from the fact that whereas the sum SINR maximization would require an exhaustive search for all possible beams and all users in the cell, the sum SLNR can be maximized by simply maximizing the SLNR of each UE.

c) Matched filter precoder [17]: The MF, also known as conjugate beamforming, maximizes the power of the received signal, without any interference consideration. It is optimum when the noise power received by the UE is much stronger than the interference that would result from the transmitted signals intended to be received by the co-scheduled UEs. For this reason, it is optimum for noise-limited scenarios.⁴ Its precoding matrix is expressed as

$$\mathbf{W}^{(\text{MF})} = \hat{\mathbf{H}}. \quad (8)$$

The gNB computes the precoding matrix after estimating the channel so as to direct the useful energy in the direction of each UE. In our evaluation, we assume complete knowledge of the channel and we use this assumption for the calculation of this and the next precoders.

d) Zero-forcing precoder: An evolution of MF linear processing can be used to limit the detrimental effects of multi-user interference. The ZF precoder tries to cancel the power of the interference, and therefore is an optimal solution for interference-limited scenarios. This interference canceling

³This principle is an assumption adopted for this evaluation. Different codebook designs can also be applied in our optimization.

⁴Noise-limited and interference-limited scenario refer, respectively, to the case in which the noise power is greater than the interference power and vice-versa.

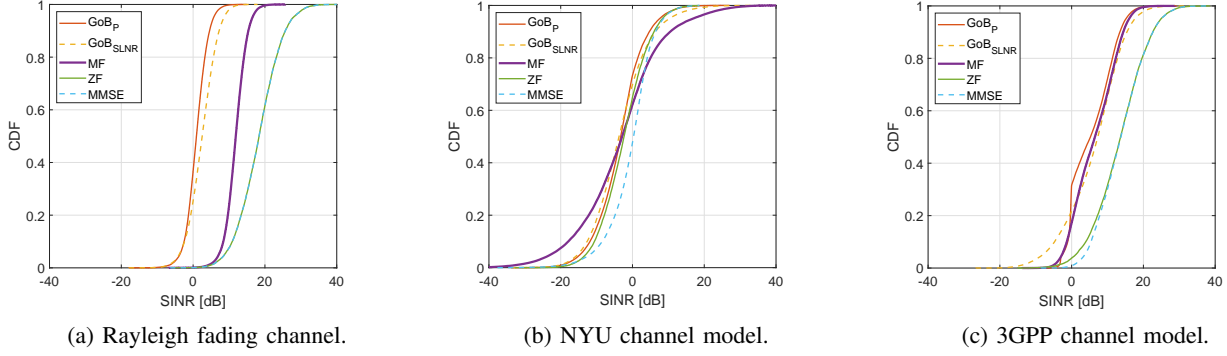


Figure 2: Empirical CDF of the SINR for the different precoders evaluated. In these figures, we used a fixed number of UEs $M = 4$ and $P_T = 30$ dBm.

property is obtained at the price of a slightly complex precoder computation and of a reduced received power. The precoding matrix is designed according to the ZF criterion [18] and is given by

$$\mathbf{W}^{(ZF)} = \hat{\mathbf{H}}(\hat{\mathbf{H}}^H \hat{\mathbf{H}})^{-1} \quad (9)$$

which simply denotes the right pseudo-inverse of the matrix $\hat{\mathbf{H}}^H$.

e) MMSE precoder: Differently from the last two precoders considered, the MMSE precoding strategy (also known as Kalman filter precoder) maximizes the sum of the SINR. Therefore, it optimizes the received power while minimizing the interference signal. It can be considered as a solution in between the MF and the ZF precoders. The precoding matrix is expressed as

$$\mathbf{W}^{(MMSE)} = \hat{\mathbf{H}} \left(\hat{\mathbf{H}}^H \hat{\mathbf{H}} + \frac{1}{\text{SNR}} \mathbf{I}_M \right)^{-1} \quad (10)$$

and it is possible to prove that it can be expressed as a linear combination of MF and ZF precoders [19].

C. Imperfect channel estimate

Focusing on a realistic system, achieving a complete and correct knowledge of the CSI is not feasible in a practical framework. To be precise, typical mmWave implementation does not have direct access to the signals received on each gNB antenna, so learning the channel on each antenna element is currently extremely difficult and almost infeasible. For this reason, we consider the performance in case the transmitter has an imperfect channel estimate. The channel estimation error is modeled following a Gauss-Markov formulation, where the imperfect channel \mathbf{H}_e is obtained using the *true* channel \mathbf{H} as follows

$$\mathbf{H}_e = \tau \mathbf{H} + \sqrt{1 - \tau^2} \mathbf{E} \quad (11)$$

where each term of the matrix \mathbf{E} follows a circularly symmetric Normal distribution $\mathcal{CN}(0,1)$. Moreover, the scalar parameter $\tau \in [0,1]$ is used to indicate the quality of the channel estimation, where $\tau = 1$ corresponds to perfect estimation of the channel whereas $\tau = 0$ corresponds to having only the random channel \mathbf{E} [20]. This parameter depends on factors such as the time/power spent on pilot-based channel estimation. As done in (3), and with the imperfect channel

Table I: List of parameters used in our evaluation. Unless specified otherwise, these settings are considered as default in all the studies carried out during our evaluation.

Value	Meaning and (Notation)
28 GHz	carrier frequency (f)
7 dB	noise figure (NF)
100 m	transmitter receiver distance
4	# of served UEs (M)
64	total # of antennas per gNB (N_T)
$[8 \times 8]$	vertical and horizontal UPA configuration
$\lambda[0.7, 0.5]$	vertical and horizontal UPA element spacing
30 dBm	transmitted power (P_T)
6	# bits phase shifters
0.99	imperfect channel metric (τ) ⁵

consideration, the equivalent matrix becomes $\bar{\mathbf{H}}_e = \hat{\mathbf{H}}^H \hat{\mathbf{W}}_e^{(p)}$, where the precoder $\hat{\mathbf{W}}_e^{(p)}$ has been calculated considering the imperfect channel \mathbf{H}_e .

III. COMPARISON RESULTS

In this section we provide some simulation results to compare the performance of the different precoders considered, which will be assessed in terms of SINR and achievable system capacity. Before examining in detail all the results, we briefly report here the SINR expression used in our evaluation. Furthermore, Table I details all the parameters and respective values adopted.

The first metric considered in our evaluation is the SINR, we calculate it for each UE m as follows

$$\text{SINR}_m^{(p)} = \frac{|\bar{\mathbf{h}}_{m,m}^{(p)}|^2}{\frac{1}{\text{SNR}} + \sum_{i \neq m} |\bar{\mathbf{h}}_{m,i}^{(p)}|^2} \quad (12)$$

where SNR is computed using the transmitted power, the path loss ℓ , and the thermal noise σ^2 as $\frac{P_T \ell^{-1}}{\sigma^2}$. We note that each UE's SINR is affected by the accurate antenna array radiation pattern that is computed considering the field factor term into the channel gains, as previously described in (4). Finally, superscript (p) is used to identify the $M \times 1$ vector of the equivalent matrix $\bar{\mathbf{H}}^{(p)}$ obtained with the corresponding precoder $\hat{\mathbf{W}}^{(p)}$. We recall that the precoding matrix is included into the equivalent matrix as done in (3).

⁵The value $\tau = 0.99$ identifies an optimistic channel imperfection. As discussed later in the results, even with a small error in the CSI the degradation is notable.

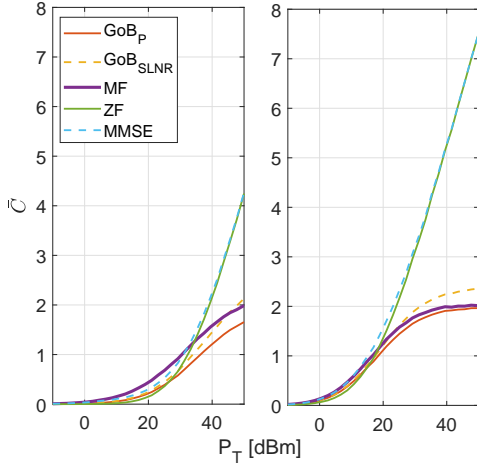


Figure 3: System capacity for the different precoders, varying the transmitted power P_T . In this figure, $M = 4$, $NF = 7$ dB, and the channel is modeled as NYU in the left plot and following the 3GPP characterization in the right plot.

The first result is a comparison of the SINR values for all the precoders studied under different channel model assumptions. In order to have a comprehensive view of the overall performance, Figure 2 reports the empirical Cumulative Distribution Function (CDF) of the SINR for all the configurations considered. The results have been collected over a sufficient number of repetitions in order to obtain the desired accuracy, thus precisely evaluating the different precoders. We compare both the NYU and 3GPP channel characterizations with a random Rayleigh channel model computed as $\mathbf{H}_R \sim \frac{1}{\sqrt{M}}\mathcal{CN}(\mathbf{0}_{N_T \times M}, \mathbf{1}_{N_T \times M})$. The figures are obtained with a Monte Carlo approach which generates random samples of channel and environment for all the UEs in each iteration. As expected, the MMSE precoder outperforms all the other configurations for most of the UEs. Furthermore, due to the high directivity of the NYU channel, both GoB precoders are able to reach higher SINR values, with respect to the MF, for more than forty percent of the UEs. We note that for this plot we have used a 7 dB noise figure⁶, which corresponds to a mostly interference-limited system [21]. Due to lack of space, we are not reporting here any results with higher noise power. However, larger noise values push the system into a noise-limited regime, hence reducing the performance of the ZF precoder.

Figure 2 also highlights the lack of fairness among UEs when the MF precoder is used. Even if the average value of MF's SINR is the highest, really high values of SINR are obtained only for a small percentage of UEs. As we can see in Figure 2a, the precoders which do not require knowledge of the channel (e.g., GoB_P and GoB_SLNR) are unable to operate efficiently when the channel is Rayleigh. Conversely, they show SINR values close to those of MF when the channel is modeled following the NYU characterization. This stems from the fact that, while a Rayleigh channel is *isotropic* and scatters

⁶The noise figure term quantifies the degradation of the Signal to Noise Ratio (SNR) due to the noise present in the system.

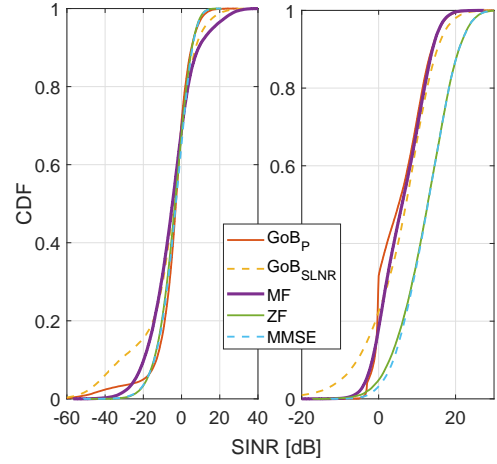


Figure 4: Empirical CDF of the SINR for the different precoders evaluated when an imperfect channel is considered. In this figure, $M = 4$, $NF = 7$ dB and $\tau = 0.99$, and the channel is modeled as NYU in the left plot and following the 3GPP characterization in the right plot.

the power without a preferred direction, realistic mmWave channels present limited multi-paths and rays with a large portion of the power concentrated in few directions. To further support such interpretation, Figure 2b reports the SINR values under NYU and 3GPP UMa channel characterizations. We note that, since the NYU model has fewer clusters than its UMa counterpart, the power is concentrated in fewer directions and thus the GoB approaches have even higher performance.

With the use of the SINR expression in (12), we can compute the channel capacity as follows

$$C_m^{(p)} = \log_2 \left(1 + \text{SINR}_m^{(p)} \right). \quad (13)$$

This metric can be used to evaluate the spectral efficiency of each configuration, and we indicate its average value by \bar{C} . Figure 3 plots the average system capacity in the different configurations as a function of the transmit power P_T used at the gNB side. The growing transmit power increases at the same rate the received power and the interference levels for the interference-blind precoders (i.e., MF, GoB) hence resulting in a saturation of the performance. Conversely, interference-aware precoders such as ZF and MMSE can have indefinitely growing performance. The figures display the good performance of the GoB precoder when the SLNR is optimized. We remark that, even if the average MF SINR is higher with respect to the other configurations, it presents poor fairness as previously discussed.

Comparing the two realistic models, we can notice also in these figures how the directivity of the NYU model results in good outcomes for the capacity in the two GoB approaches in the range of values around 20 dBm of transmitted power. Contrary to expectation, in this particular range, GoB procedures can perform appreciably better than ZF if high spectral efficiency is desired, while, if a more energy-efficient operating point is chosen, the performance gap narrows, and eventually MF outperforms all the other configurations.

As the last result, Figure 4 reports the empirical CDF of the

Table II: Evaluation of the gaps in the 50th percentile of the SINR expressed in dB for the different precoders considered in this evaluation. Table obtained with a fixed number of UEs $M = 4$, and $P_T = 30$ dBm.

	perfect CSI ($\tau = 1$)		imperfect CSI ($\tau = 0.99$)	
	NYU	3GPP	NYU	3GPP
MF – GoB _{SLNR}	+0.87	−0.80	−0.46	−1.03
ZF – GoB _{SLNR}	+1.40	+6.33	+0.89	+5.67
MMSE – GoB _{SLNR}	+4.05	+6.45	+1.36	+5.67

SINR when an imperfect channel \mathbf{H}_e is considered. Comparing it with Figure 2, is it possible to notice how the imperfection in the CSI results in a degradation of the performance, especially for the linear precoders. More importantly, when an error in the channel estimation is considered, the gap between GoB optimization approaches and linear precoders is strongly reduced and, in most cases, GoB is even able to outperform the linear precoders. We recall that gathering the CSI necessary to use MF, ZF and the MMSE precoders has a cost for the system that should be properly considered. Furthermore, given the small implementation loss of GoB precoding with respect to more refined systems, and considering the high level of complexity that gathering the necessary CSI would require, it seems that the additional complexity may not be justified by the modest (or even vanishing) performance improvement.

Remarks: We report in this subsection the main remarks raised in our evaluation study. Due to the directionality of mmWave channels, our results support GoB approaches as a good trade-off between CSI acquisition complexity and performance. Given the limited advantage (about +4 dB with MMSE and the NYU channel model), there is no strong motivation to use linear precoders in multi-user systems at mmWave frequencies. Table II summarizes our findings, reporting the SINR gaps for the 50th percentile in the different approaches considered. Although linear precoders can exploit a larger amount of information on the channel matrix, requiring full CSI at the transmitter, the gain under imperfect CSI can be assessed as less than +1.36 dB with MMSE and the NYU channel model. If the inaccuracy of the channel estimation grows, it is possible to conjecture that the gap would close even more, eventually eliding any advantage. A similar trend, though with slightly higher gains, can be observed when the 3GPP channel model is considered.

IV. CONCLUSION AND FUTURE WORKS

In this study, we have highlighted the impact of realistic mmWave channel behaviors on the downlink mmWave MU MIMO system when different precoders are considered at the gNB side. Our study led to the following observations. Under ideal condition (i.e., Rayleigh channel model, perfect CSI), linear precoders largely outperform GoB due to their ability to perfectly adapt to the channel realization. However, the directionality present in realistic channel models reduces the gap, sometimes even letting the GoB approaches surpass more complex solutions and in most cases not justifying the additional complexity.

Finally, we have studied how the performance behaves when considering an error in the CSI acquisition. Results show that, even with a small CSI imprecision, the performance gap between linear precoding and GoB vanishes.

The study of more refined MMSE approaches which include per-user power balancing, as well as a theoretical evaluation of the performance of the various techniques, also for different frequency bands, are left for future study.

REFERENCES

- [1] Cisco, “Cisco Visual Networking Index: Global Mobile Data Traffic Forecast Update, 2016–2021,” *White Paper*, March 2017.
- [2] S. Rangan, T. S. Rappaport, and E. Erkip, “Millimeter-Wave Cellular Wireless Networks: Potentials and Challenges,” *Proceedings of the IEEE*, vol. 102, no. 3, pp. 366–385, March 2014.
- [3] E. G. Larsson, O. Edfors, F. Tufvesson, and T. L. Marzetta, “Massive MIMO for next generation wireless systems,” *IEEE Communications Magazine*, vol. 52, no. 2, pp. 186–195, February 2014.
- [4] H. Yang and T. L. Marzetta, “Performance of Conjugate and Zero-Forcing Beamforming in Large-Scale Antenna Systems,” *IEEE J. Sel. Areas Commun.*, vol. 31, no. 2, pp. 172–179, February 2013.
- [5] J. Hoydis, S. ten Brink, and M. Debbah, “Massive MIMO in the UL/DL of Cellular Networks: How Many Antennas Do We Need?” *IEEE J. Sel. Areas Commun.*, vol. 31, no. 2, pp. 160–171, February 2013.
- [6] D. L. Colon, F. H. Gregorio, and J. Cousseau, “Linear precoding in multi-user massive MIMO systems with imperfect channel state information,” in *XVI Workshop on Information Processing and Control (RPIC)*, Oct 2015, pp. 1–6.
- [7] X. Gao, O. Edfors, F. Rusek, and F. Tufvesson, “Linear Pre-Coding Performance in Measured Very-Large MIMO Channels,” in *IEEE Vehicular Technology Conference (VTC Fall)*, Sept 2011, pp. 1–5.
- [8] M. E. Hassan, A. E. Falou, and C. Langlais, “Performance assessment of linear precoding for multi-user massive MIMO systems on a realistic 5G mmWave channel,” in *IEEE Middle East and North Africa Communications Conference (MENACOMM)*, April 2018.
- [9] 3GPP, “TS 38.104 Base Station radio transmission and reception,” 2018.
- [10] —, “TS 38.211, Physical Channels and Modulation,” 2018.
- [11] —, “TS 38.214, Physical layer procedures for data,” 2018.
- [12] —, “TS 37.840 Group Radio Access Network; Study of Radio Frequency and Electromagnetic Compatibility requirements for Active Antenna Array System base station,” 2013.
- [13] M. Akdeniz, Y. Liu, M. Samimi, S. Sun, S. Rangan, T. Rappaport, and E. Erkip, “Millimeter Wave Channel Modeling and Cellular Capacity Evaluation,” *IEEE J. Sel. Areas Commun.*, vol. 32, no. 6, pp. 1164–1179, June 2014.
- [14] 3GPP, “TS 38.900 Group Radio Access Network; Study on channel model for frequency spectrum above 6 GHz,” 2016.
- [15] P. Kyosti et al., “WINNER II channel model,” *Technical Report IST-WINNER D1.1.2 ver 1.1*, Sept. 2007.
- [16] M. Rebato, L. Resteghini, C. Mazzucco, and M. Zorzi, “Study of Realistic Antenna Patterns in 5G mmWave Cellular Scenarios,” in *IEEE Int. Conf. Commun., Reliability and Modeling Symposium*, Kansas City, USA, May 2018.
- [17] M. Joham, W. Utschick, and J. A. Nossek, “Linear transmit processing in MIMO communications systems,” *IEEE Trans. Signal Process.*, vol. 53, no. 8, pp. 2700–2712, Aug 2005.
- [18] C. B. Peel, B. M. Hochwald, and A. L. Swindlehurst, “A vector-perturbation technique for near-capacity multiantenna multiuser communication-part I: channel inversion and regularization,” *IEEE Trans. Commun.*, vol. 53, no. 1, pp. 195–202, Jan 2005.
- [19] L. Rose and M. Maso, “Receiver-Centric Inter-Cell Interference Cancellation in D2D-Assisted Networks,” in *IEEE Globecom Workshops*, Dec 2016.
- [20] A. Müller, A. Kammoun, E. Björnson, and M. Debbah, “Efficient linear precoding for massive MIMO systems using truncated polynomial expansion,” in *IEEE 8th Sensor Array and Multichannel Signal Processing Workshop (SAM)*, June 2014, pp. 273–276.
- [21] M. Rebato, M. Mezzavilla, S. Rangan, F. Boccardi, and M. Zorzi, “Understanding Noise and Interference Regimes in 5G Millimeter-Wave Cellular Networks,” in *22th European Wireless Conference*, May 2016.